https://doi.org/10.1016/j.renene.2021.09.024 **This is the Pre-Published Version.**

# Damage identification of wind turbine blades using an adaptive method for compressive beamforming based on the generalized minimax-concave penalty function

Shilin Sun[a], Tianyang Wang[a,*], Hongxing Yang[b], Fulei Chu[a]

[a]*Department of Mechanical Engineering, Tsinghua University, Beijing 100084, China*

[b]*Renewable Energy Research Group (RERG), Research Institute for Sustainable Urban Development, The Hong Kong Polytechnic University, Hong Kong*

## Abstract

Wind turbine blades are critical components in wind energy generation, and blade health management is a challenging issue for the operation and maintenance of wind turbines. In this paper, an adaptive method is developed to identify blade damages based on the microphone array and compressive beamforming, and global and remote health assessment can be accomplished. In this method, the generalized minimax-concave penalty function is employed to enhance sparse recovery capacities, and step-sizes in computation processes are adjusted adaptively to adapt to variational conditions. Besides, potential damage locations are extracted in coarse acoustic maps to improve convergence rates. Numerical simulations show that high spatial resolutions can be achieved by the proposed method, and the computation time for solving acoustic inverse problems is less than using existing algorithms, especially with low-frequency sources. Moreover, experiments are conducted with a small-scale wind turbine. Results demonstrate that several damages in operating blades can be precisely recognized with high efficiencies, and the deterioration of acoustic maps induced by improper step-sizes can be avoided. The proposed method provides a promising way for in-situ health monitoring of wind turbine blades.

**Keywords**: wind turbine blade; damage identification; microphone array; beamforming; structural health monitoring

## 1. Introduction

Wind energy, as one of the promising and renewable energy sources, has experienced dramatic development for decades all over the world [1]. According to the report from the International

* Corresponding author. Tel. /Fax: 86-10-62790532
Email address: wty19850925@126.com (Tianyang Wang).

Energy Agency, there is a steady growth trend in wind energy exploitation, and wind energy generation is predicted to reach 4000 TW·h in 2030 [2-3]. In addition, the global goal of sustainable development is expected to be achieved with the utilization of wind energy.

Wind turbine is the critical equipment for wind energy generation, and blades are crucial and expensive components in wind turbines [4]. Wind turbine blades interact with the wind directly, and they are leading parts for power generation efficiency since gearboxes and power generators are driven by blades ultimately. Moreover, wind turbine blades are usually located in high-altitude and harsh environments where wind resources are extremely abundant. Besides, there is a trend that blades are manufactured to be increasingly large [5]. In this case, the failure rate of blades is relatively high with respect to other parts in wind turbines, and both economic losses and catastrophic accidents are easily induced by undetected blade damages [6]. Hence, it is necessary to recognize damages in wind turbine blades, which can reduce operation and maintenance costs and improve the reliability of wind energy generation. With accurate monitoring of blade health conditions, serious accidents can be avoided by repairing or replacing damaged blades in time, and power generation losses caused by downtime can be reduced [7-8].

Several techniques have been proposed to identify damages in wind turbine blades. Ultrasonic and radiographic inspections are restricted to be used in manufacturing processes due to the limitation of scanning distances and coupling agents [9-10]. Vibration measurement is widely used in fault diagnosis of gearboxes [11-12], and it has also been applied to detect damages in wind turbine blades [13-14]. However, the identification of local damages in blades is hard to be achieved by vibration-based methods. Strain measurement can be accomplished using strain gauges and fiber Bragg gratings, and the sensing range is inadequate since structural deflections are small away from damage sources [15-16]. The main challenge of blade damage identification lies in the difficulty of damage characterization at the global level; thus, spatial information is necessary for health assessment. Microphone array is a useful facility for spatial filter and source recognition with acoustic maps, and it has been extensively used in speech enhancement [17] and noise localization [18]. Recently, a blade health monitoring scheme based on the microphone array has been studied [19], and blade damages can be actively detected by installing loudspeakers in internal cavities. In this case, structural damages are possible to be identified by externally positioned microphone array, since sound transmission properties across blade walls are affected by structural integrities.

Moreover, this scheme has the potential to be applied for operating blades due to the broad sensing range and convenience of damage localization. The schematic of the damage identification technique is depicted in Fig. 1. With excitations of loudspeakers, the microphone array is expected to recognize blade damages remotely [20], which is beneficial to reduce casualty accidents and power losses induced by blade failures. However, there are several unresolved problems in the current research for reliable inspections. Specifically, the spatial resolution in acoustic maps is inadequate to extract valid features of blade damages, and health monitoring applicability for operating blades has not been investigated in experiments.

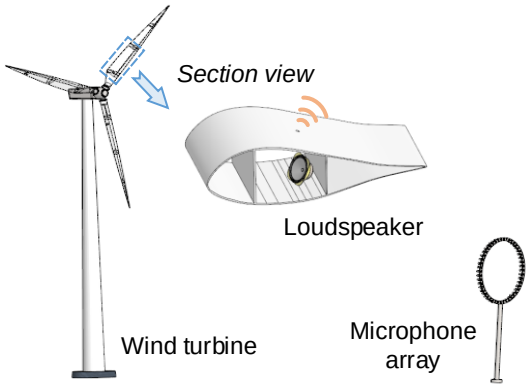


**Fig. 1.** Schematic of blade damage identification with the microphone array.

Beamforming is the key technique for identifying acoustic sources with the microphone array, and conventional beamforming is the most widely used method [21]. Spatial resolution of the conventional beamforming is restricted by the Rayleigh criterion, and source strength estimations are inaccurate when multiple damages exist in blades [22]. Compressive beamforming has been proposed to reconstruct sound fields by solving acoustic inverse problems with sparse prior information, and it has been applied to ocean acoustic measurement [23] and noise detection [24]. It is reported that the spatial resolution of compressive beamforming is much higher than the conventional beamforming and the deconvolution methods [25]. For blade damage identification with the microphone array, acoustic sources are sparse since damages that are hard to be examined by traditional methods are usually in infancies. The underlying sparsity brings the possibility to identify blade damages based on compressive beamforming. One of the well-known compressive beamforming strategies is $l_1$-norm minimization, by which the underestimation of source strengths is unavoidable due to the penalty unevenness, and it may fail to recognize sources with insufficient sparsity [23, 26]. The weakness of $l_1$-norm minimization prevents its application for blade health monitoring, especially with distributed damages. An alternative to $l_1$-norm for sparse regularization

is the generalized minimax-concave (GMC) penalty function, by which the homogeneity of penalties to non-zero elements can be employed to improve sparse recovery accuracies [27-28]. However, there exist difficulties in the utilization of the GMC penalty function for blade damage identification with the microphone array. Specifically, the proper step-size in solving procedures of acoustic inverse problems with GMC penalties is hard to be determined due to the complexity of operating conditions. To improve the reliability of identification results, a small value of step-size should be used, while the large one is beneficial to reduce the computation time. With inappropriate step-sizes, blade damages could be wrongly recognized in blurry acoustic maps, and the high computation efficiency is difficult to be guaranteed. Therefore, there is an urgent demand to develop applicable methods for blade damage identification based on compressive beamforming and GMC penalties, which is promising to evaluate blade health conditions in actual scenarios.

In this investigation, compressive beamforming is considered in structural health monitoring of wind turbine blades for the first time, and an adaptive method is proposed to generate high-quality acoustic maps efficiently for blade damage identification. Specifically, residual of sound field reconstruction is regularized by GMC penalties to improve the recognition performance for acoustic sources corresponding to blade damages. Besides, acoustic inverse problems are solved by the proximal gradient method (PGM) with backtracking and acceleration strategies, and proximal gradient steps are implemented at extrapolation points with adaptively adjusted step-sizes. In this case, step-sizes are large during the initial period to accelerate the convergence, and small step-sizes are adopted at the later stage to improve damage identification precisions. Moreover, auxiliary information about potential damage locations is exacted by conventional beamforming and peak search procedures to enhance computational efficiencies. The proposed method is robust since the step-size limitation in the existing algorithm [27] for guaranteeing convergence can be removed by adjusting step-sizes adaptively.

The rest of this paper is organized as follows: Section 2 provides basic theories about acoustic inverse problems, convex optimization, peak search, and the proposed method. Then, Monte Carlo simulation results based on different methods are analyzed in Section 3. In addition, Section 4 shows experimental validations of the proposed method for damage identification. Finally, conclusions are presented in Section 5.

## 2. Basic theories

### 2.1 Compressive beamforming

Let us refer to an array consisting of $M$ microphones, which are placed at $\boldsymbol{r}_m$ ($m$ = 1, 2, …, $M$). Suppose that the search region is divided into $N$ grid points, and the position of each point is denoted as $\boldsymbol{r}_n$ ($n$ = 1, 2, …, $N$). When there is no flow, the acoustic inverse problem in the frequency domain is denoted as

$$\boldsymbol{p} = \boldsymbol{G}\boldsymbol{q} + \boldsymbol{e} \tag{1}$$

where $\boldsymbol{p} = [p_1, p_2, \ldots, p_M]^{\mathrm{T}}$ is the sound pressure vector, $\boldsymbol{q} = [q_1, q_2, \ldots, q_N]^{\mathrm{T}}$ is the potential source strength vector, $\boldsymbol{e} = [e_1, e_2, \ldots, e_M]^{\mathrm{T}}$ is the noise vector, $\boldsymbol{G}$ is the propagation matrix consisting of the transfer function $g_{mn} = \dfrac{1}{4\pi|\boldsymbol{r}_m - \boldsymbol{r}_n|}\mathrm{e}^{-\mathrm{j}\frac{\omega_n}{c}|\boldsymbol{r}_m - \boldsymbol{r}_n|}$, $\omega_n$ is the angular frequency, $c$ is the velocity of sound, and $\mathrm{j} = \sqrt{-1}$ is the imaginary unit.

The basic principle for compressive beamforming is to identify acoustic sources by solving inverse problems with sparse prior information. Compressive beamforming based on the GMC penalty function estimates $\boldsymbol{q}$ from Eq.(1) using a fine approximation of $l_0$-norm, and acoustic maps are generated based on the optimization problem

$$\min_{\boldsymbol{q}}\left[\frac{1}{2}\left\|\boldsymbol{p} - \boldsymbol{G}\boldsymbol{q}\right\|_2^2 + \lambda\psi_{\boldsymbol{B}}(\boldsymbol{q})\right] \tag{2}$$

where $\lambda > 0$ is the regularization parameter, $\psi_{\boldsymbol{B}}(\boldsymbol{q}) = \left\|\boldsymbol{q}\right\|_1 - H_{\boldsymbol{B}}(\boldsymbol{q})$ is the GMC penalty function, and $H_{\boldsymbol{B}}(\boldsymbol{q}) = \min_{\boldsymbol{v}}\left[\left\|\boldsymbol{v}\right\|_1 + \frac{1}{2}\left\|\boldsymbol{B}(\boldsymbol{q} - \boldsymbol{v})\right\|_2^2\right]$ is the generalized Huber function.

By considering the auxiliary variable $\boldsymbol{v}$, Eq.(2) can be expressed as a saddle-point problem

$$\min_{\boldsymbol{q}}\max_{\boldsymbol{v}} F(\boldsymbol{q}, \boldsymbol{v}) \tag{3}$$

where $F(\boldsymbol{q}, \boldsymbol{v}) = \frac{1}{2}\left\|\boldsymbol{p} - \boldsymbol{G}\boldsymbol{q}\right\|_2^2 + \lambda\left\|\boldsymbol{q}\right\|_1 - \lambda\left\|\boldsymbol{v}\right\|_1 - \frac{\lambda}{2}\left\|\boldsymbol{B}(\boldsymbol{q} - \boldsymbol{v})\right\|_2^2$.

With the reasonable selection of key parameters including $\lambda$ and $\boldsymbol{B}$, the objective function can be convex even though the penalty function is non-convex [27]. Hence, the non-convexity can be used to generate more accurate results for blade damage identification than using $l_1$-norm minimization, and the inverse problem can be solved by convex optimization [29].

### 2.2 Proximal gradient method

PGM is a powerful approach for non-smooth optimization, and the fundamental idea is to split

the objective function into two items, one of which is differentiable [30]. In this condition, the objective function in Eq.(3) with respect to variable $\boldsymbol{q}$ is expressed as

$$F(\boldsymbol{q}) = f_1(\boldsymbol{q}) + f_2(\boldsymbol{q}) \tag{4}$$

where $f_1(\boldsymbol{q}) = \frac{1}{2}\|\boldsymbol{p} - \boldsymbol{G}\boldsymbol{q}\|_2^2 - \lambda\|\boldsymbol{v}\|_1 - \frac{\lambda}{2}\|\boldsymbol{B}(\boldsymbol{q} - \boldsymbol{v})\|_2^2$ denotes the smooth item and $f_2(\boldsymbol{q}) = \lambda\|\boldsymbol{q}\|_1$ denotes the non-smooth item.

PGM is performed with proximal gradient steps, and the variable update rule is

$$\boldsymbol{q}^{(k+1)} = \mathbf{prox}_{\eta f_2}\left[\boldsymbol{q}^{(k)} - \eta\nabla f_1\left(\boldsymbol{q}^{(k)}\right)\right] \tag{5}$$

where **prox** is the proximal operator, $k$ is the counting variable, $\eta$ is the step-size, and $\nabla f$ denotes the gradient of function $f$ [31].

PGM converges with a rate of $O\left(\frac{1}{k}\right)$ when $\eta \in \left(0, \frac{1}{L}\right]$ and $\nabla f$ is Lipschitz continuous with a constant $L$ [30]. Nevertheless, convergence is merely the fundamental requirement for blade damage identification, and the computation precision and efficiency are affected by the selection of step-sizes. In actual operations, characteristics of wind turbines and circumstances are variational, and the determination of step-sizes is a challenging matter for the array-based methods. To handle this problem, the backtracking strategy can be utilized to adjust step-sizes adaptively [32]. Hence, a large value can be set as the initial step-size, then the Lipschitz condition is examined repeatedly to decrease the step-size with the shrinkage factor $0 < \beta < 1$. The PGM solving process continues only if the following condition is satisfied

$$f_1(\boldsymbol{q}') \le f_{1\eta}\left(\boldsymbol{q}', \boldsymbol{q}^{(k)}\right) \tag{6}$$

where $\boldsymbol{q}' = \mathbf{prox}_{\eta f_2}\left[\boldsymbol{q}^{(k)} - \eta\nabla f_1\left(\boldsymbol{q}^{(k)}\right)\right]$ and $f_{1\eta}\left(\boldsymbol{q}', \boldsymbol{q}^{(k)}\right) = f_1\left(\boldsymbol{q}^{(k)}\right) + \nabla f_1\left(\boldsymbol{q}^{(k)}\right)^{\mathrm{T}}\left(\boldsymbol{q}' - \boldsymbol{q}^{(k)}\right) + \frac{1}{2\eta}\left\|\boldsymbol{q}' - \boldsymbol{q}^{(k)}\right\|_2^2$.

Furthermore, the convergence efficiency of PGM can be improved by the acceleration strategy [33]. In detail, each proximal gradient step for $k > 0$ is conducted at the extrapolation point

$$\boldsymbol{y}^{(k)} = \boldsymbol{q}^{(k)} + \rho^{(k)}\left(\boldsymbol{q}^{(k)} - \boldsymbol{q}^{(k-1)}\right) \tag{7}$$

where $\rho^{(k)} = \frac{\theta_k - 1}{\theta_{k+1}}$ is the extrapolation parameter, the scale factor $\theta_k^2 = \theta_{k+1}^2 - \theta_{k+1}$, and $t_0 = 1$.

It has been proven that iteration times for accelerated PGM to obtain the $\varepsilon$-optimal solution is $\left\lceil \sqrt{\frac{2\eta L\left\|\boldsymbol{q}_0 - \boldsymbol{q}^*\right\|_2^2}{\varepsilon}} - 1 \right\rceil$ at most, while that for original PGM is $\left\lceil \frac{\eta L\left\|\boldsymbol{q}_0 - \boldsymbol{q}^*\right\|_2^2}{2\varepsilon} \right\rceil$, where $\boldsymbol{q}_0$ is the initial solution, and $\boldsymbol{q}^*$ is the optimal solution [34].

### 2.3 Peak search

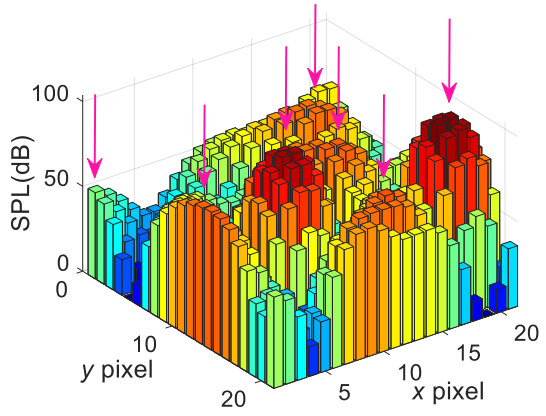


**Fig. 2.** Illustration of peaks in an acoustic map.

Fig. 2 shows a rough acoustic map generated by conventional beamforming, in which several peaks indicating potential damages in blades are marked by downward arrows. It is shown that peaks in the acoustic map distribute among a number of connected grids due to the low spatial resolution. Thus, peak detection cannot be accomplished by the pixel-by-pixel search directly. Moreover, there are similarities between the peak and Gaussian function with respect to the shape, providing opportunities to extract peaks by template matching. In this paper, peaks in acoustic maps are recognized using two-dimensional Gaussian function

$$f(x,y)=\frac{1}{2\pi\sigma_x\sigma_y}\mathrm{e}^{-\left[\frac{(x-\mu_x)^2}{2\sigma_x^2}+\frac{(y-\mu_y)^2}{2\sigma_y^2}\right]} \tag{8}$$

where $\mu_x$ and $\mu_y$ denote means, and $\sigma_x$ and $\sigma_y$ are standard deviations.

With proper parameters in Eq.(8), the Gaussian function can be adjusted to have a similar shape with peaks in acoustic maps. Thus, it is feasible to find peaks by filtering acoustic maps with the Gaussian kernel function, and the extraction can be achieved using two-dimensional convolution. Then, the pixel-by-pixel search is used to locate peaks in filtered results, in which the value of each pixel represents the similarity between the surrounding region and kernel function.

### 2.4 The proposed method for blade damage identification

In the damage identification of wind turbine blades with the microphone array, potential damages are represented by sources in acoustic maps, and health evaluation accuracies are closely correlated to acoustic source recognition performances. Compressive beamforming based on the GMC penalty function is superior in improving spatial resolutions while the computation is time-

consuming, and conventional beamforming is efficient for acoustic source recognition. Hence, there is a potential to achieve satisfactory performances of both efficiency and accuracy with the combination of conventional beamforming and compressive beamforming. Blade damages mainly exist in regions where acoustic source strengths are higher than surrounding areas, and they are relevant to peaks in acoustic maps. In this case, with the recognition of peaks from conventional beamforming results, a well-designed initial solution can be formed based on auxiliary information concerning potential damage locations. Compared to widely used initial solutions, including random values and zeros, the solution initialization pattern enhances the similarity between initial and target solutions further. Therefore, the convergence rate can be improved by decreasing iterative steps used to estimate the distribution of supports in damage identification results.

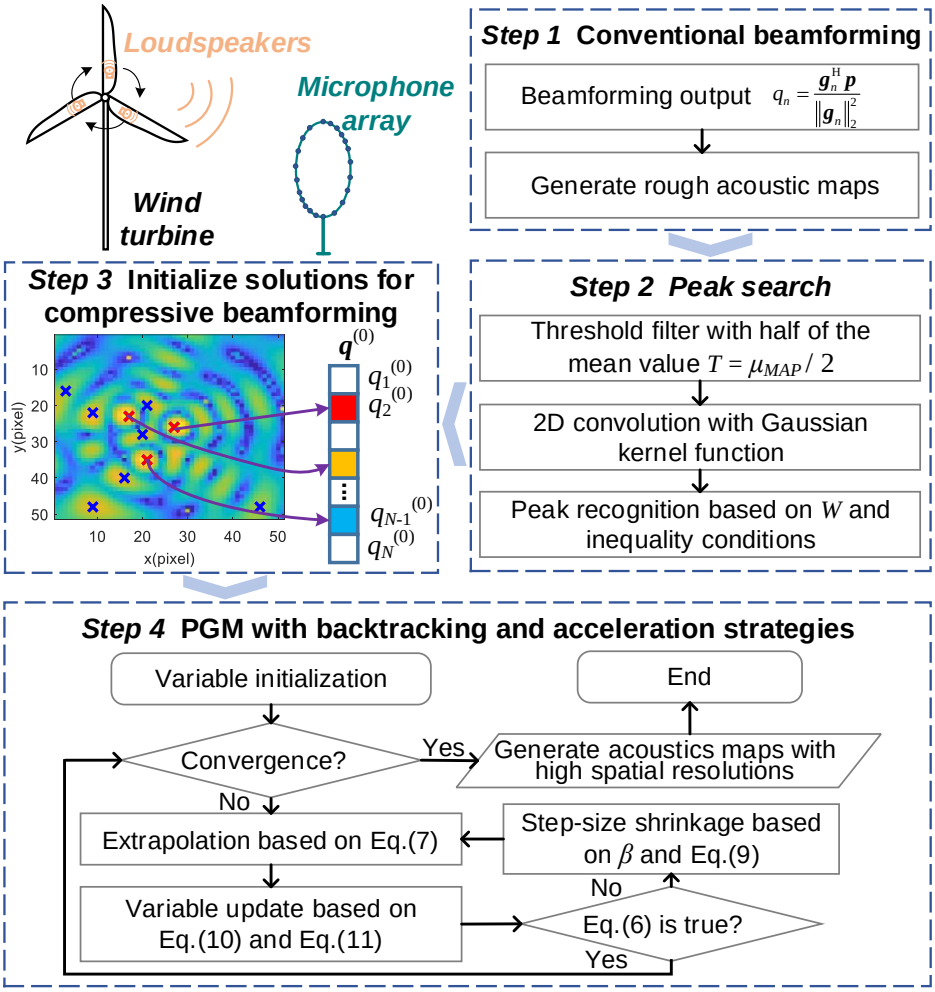


**Fig. 3.** Flowchart of the proposed method.

Moreover, the solving stability and efficiency of acoustic inverse problems with GMC penalties can be improved by backtracking and acceleration strategies. Specifically, adaptively adjusted step-sizes are used to avoid inappropriate iteration processes, and the extrapolation based

on two previous points is adopted to accelerate the convergence of proximal gradient steps. Thus, step-sizes are set to large values at the early stage to approach the vicinity of desired results rapidly, and solutions are finely tuned with small step-sizes at last to guarantee the identification accuracy of blade damages. In this case, there is no difficulty to estimate the proper value of step-sizes before solving processes, and the step-size can be set to a relatively large value without the consideration of the Lipschitz constant.

Hence, a novel and adaptive method is developed to identify blade damages based on acoustic maps with high spatial resolutions and efficiencies. The flow chart of the proposed algorithm is shown in Fig. 3, and the primary steps are summarized as follows:

***Step 1***: For a $M$-tuple array measurement $\boldsymbol{p}$, the rough acoustic map $\boldsymbol{Q} = [Q_{r,s}]_{R\times S}$ ($r$ = 1, 2, …, $R$, $s$ = 1, 2, …, $S$, and $R \times S = N$) is generated by conventional beamforming, in which $Q_{r,s} = 20\log_{10}\frac{q_n}{2\times10^{-5}}$, $q_n = \frac{\boldsymbol{g}_n^{\mathrm{H}}\boldsymbol{p}}{\|\boldsymbol{g}_n\|_2^2}$, $n = R(s-1)+r$, and $\boldsymbol{g}_n$ is the $n$-th column of $\boldsymbol{G}$ as described in Eq.(1).

***Step 2***: The rough acoustic map is cleaned by removing elements less than $T = \frac{\mu_{MAP}}{2}$, and $\mu_{MAP}$ denotes the mean value of map elements. Then, two-dimensional convolution is implemented with the map and Gaussian kernel function to generate the filtered map $\hat{\boldsymbol{Q}} = [\hat{Q}_{r,s}]_{R\times S}$. In addition, peaks are recognized based on inequality conditions: $\hat{Q}_{r,s} \geq \hat{Q}_{r-1,s-1}$, $\hat{Q}_{r,s} \geq \hat{Q}_{r-1,s}$, $\hat{Q}_{r,s} \geq \hat{Q}_{r-1,s+1}$, $\hat{Q}_{r,s} \geq \hat{Q}_{r,s-1}$, $\hat{Q}_{r,s} \geq \hat{Q}_{r,s+1}$, $\hat{Q}_{r,s} \geq \hat{Q}_{r+1,s-1}$, $\hat{Q}_{r,s} \geq \hat{Q}_{r+1,s}$, and $\hat{Q}_{r,s} \geq \hat{Q}_{r+1,s+1}$. Finally, locations of the first $W$ peaks in descending order are recorded as $\boldsymbol{d} = [d_1, d_2, ..., d_W]^{\mathrm{T}}$, where $d_l$ ($l$ = 1, 2, …, $W$) is the index of the $l$-th peak with respect to conventional beamforming results in the vector form.

***Step 3***: The initial solution for compressive beamforming is formed as $\boldsymbol{q}^{(0)}$, in which elements corresponding to $\boldsymbol{d}$ are set to random values, and other positions are filled with zeros.

***Step 4***: Acoustic inverse problem with the GMC penalty function is solved with $\boldsymbol{q}^{(0)}$ through iteration processes, and the step-size shrinkage factor $0 < \beta < 1$ is considered to adjust the step-size in each iteration step adaptively. Specifically, the step-size is scaled down by $\beta$ as

$$\eta_{t+1}^{(k)} = \beta\eta_t^{(k)} \tag{9}$$

where $t$ is the index of iterations for step-size adjustment, and $\eta_0^{(k)} = \eta^{(k-1)}$.

Eq.(9) is executed repeatedly until the condition in Eq.(6) is satisfied, and $\eta^{(k)} = \eta_{t+1}^{(k)}$. In

addition, optimization variables are updated as

$$\boldsymbol{q}^{(k+1)} = \arg\min_{\boldsymbol{q}} \left\{ \frac{1}{2\lambda\eta^{(k)}} \left\| \boldsymbol{q} - \boldsymbol{y}^{(k)} + \eta^{(k)} \boldsymbol{G}^{\mathrm{T}} \left[ \boldsymbol{G}\boldsymbol{y}^{(k)} + \gamma \boldsymbol{G}\left( \boldsymbol{v}^{(k)} - \boldsymbol{y}^{(k)} \right) - \boldsymbol{p} \right] \right\|_2^2 + \|\boldsymbol{q}\|_1 \right\} \tag{10}$$

$$\boldsymbol{v}^{(k+1)} = \arg\min_{\boldsymbol{v}} \left[ \frac{1}{2\lambda\eta^{(k)}} \left\| \boldsymbol{v} - \boldsymbol{v}^{(k)} + \eta^{(k)} \gamma \boldsymbol{G}^{\mathrm{T}} \boldsymbol{G}\left( \boldsymbol{v}^{(k)} - \boldsymbol{q}^{(k+1)} \right) \right\|_2^2 + \|\boldsymbol{v}\|_1 \right] \tag{11}$$

where $k$ is the counting variable for solving process, $0 < \gamma < 1$ is the balanced factor for determining $\boldsymbol{B} = \sqrt{\frac{\gamma}{\lambda}}\boldsymbol{G}$, $\eta^{(k)}$ denotes the step-size, and $\boldsymbol{y}^{(k)}$ is the extrapolation point defined in Eq.(7).

The iteration process for solving acoustic inverse problems executes until the convergence condition is satisfied, and a common criterion is the relative error between two adjacent steps.

Overall, there are two key parameters in the proposed method: potential source number $W$ and step-size shrinkage factor $\beta$. Specifically, supports in the designed initial solution are influenced by $W$, and $\beta$ adjusts the step-size in each iteration step adaptively to balance the solving efficiency and result precision. Additional computations induced by conventional beamforming and peak search are certainly marginal since there is no iteration process in them, and the proposed method provides an efficient way to identify blade damages with the superiority of GMC penalties.

## 3. Numerical studies

Before experimental verifications, several numerical simulations are implemented to investigate the effects of key parameters on performances of the proposed method, and parameter selection criteria are discussed. In addition, blade damages are simulated by a number of monopole acoustic sources in the framework of active damage identification with the microphone array. To indicate source identification accuracies quantitatively, the location relative error index (LEI) and magnitude relative error index (MEI) are defined as

$$\mathrm{LEI} = \frac{\left\| \boldsymbol{q}_{co}^{*} - \boldsymbol{q}_{co} \right\|_1}{N} \times 100\% \tag{12}$$

$$\mathrm{MEI} = \frac{\sum_{i=1}^{I} \left| \boldsymbol{q}^{*}(i) - \boldsymbol{q}(i) \right|}{\sum_{i=1}^{I} \left| \boldsymbol{q}^{*}(i) \right|} \times 100\% \tag{13}$$

where $\boldsymbol{q}^{*}$ is the actual strength vector of acoustic sources in sound pressure level (SPL); $\boldsymbol{q}$ is the computed strength vector in SPL; $\boldsymbol{q}_{co}$ denotes the copied vector of $\boldsymbol{q}$, and non-zero elements in $\boldsymbol{q}_{co}$ are set to 1; $\boldsymbol{q}(i)$ is the $i$-th element of $\boldsymbol{q}$; $N$ is the number of search grids; $I$ is the number of actual sources.

### 3.1 Effects of potential source numbers

In acoustic maps, blade damages are represented by identified sources, and the potential source number $W$ provides auxiliary information concerning supports in damage identification results. The determination of $W$ is necessary for the employment of the developed method. However, it is not easy to estimate the value of $W$ in advance since obtaining the number of damages is exactly one of the targets of blade damage identification. Hence, it is significant to examine the effects of the assumed $W$ on sound field reconstruction, especially when estimations of $W$ are away from the actual value.

Monte Carlo simulations are utilized to investigate the impacts of $W$ on computation processes and results. Specifically, the proposed method with $W$ = 1, 2, …, 9, and the incomplete method without $W$ are separately conducted 200 times with the existence of four acoustic sources, which are randomly placed in each trial to simulate blade damages. With different values of $W$, particular initial solutions are formed based on conventional beamforming results, while without $W$ means that the solution is initialized randomly. A ring array with 50 microphones is set at a distance of 0.5 m from the 0.6 m × 0.6 m reconstruction plane, in which 1681 search grids and four acoustic sources at 3000 Hz are considered. Moreover, white Gaussian noise is added to signals received by each microphone with a signal-to-noise ratio (SNR) of 25 dB. The convergence is regarded to be achieved when the relative error between two adjacent iteration steps becomes less than $10^{-3}$, and $\beta$ is 0.7 in all trials.

As shown in Fig. 4(a), the average iteration time is sufficiently relevant to $W$. When values of $W$ are close to the actual value, the average iteration time can be reduced with respect to the condition without $W$, which is represented as the red dotted line. In the ideal case, the computation efficiency is improved by 40.49% at most. This benefits from the estimation of solution supports, which are advantageous to arrange initial solutions that are similar to the desired pattern. Even when $W$ is set away from the actual value, the average iteration time is close to that of the case without $W$, indicating that the deterioration of computation efficiency with improper $W$ is avoided. In this case, solutions with wrong supports can be regarded as random vectors, and the solving efficiency is no worse than that with the latter. Fig. 4(b) depicts the cumulative distribution function (CDF) of iteration time in trials with $W$ = 4 and 8, and without $W$. The CDF reveals the probability that the iteration time is no more than the given value, and the probability is estimated by

occurrence frequencies in this segment. When $W = 4$, the probability that iteration time is less than 8 s is 96.1%, while the corresponding probabilities for conditions with $W = 8$ and without $W$ are 63.4% and 62.7%, respectively. The average LEI and MEI are illustrated in Fig. 4(c) and Fig. 4(d). It is clear that the value of $W$ has no obvious influence on source localization accuracy, and magnitude errors of source strengths are insensitive to $W$.

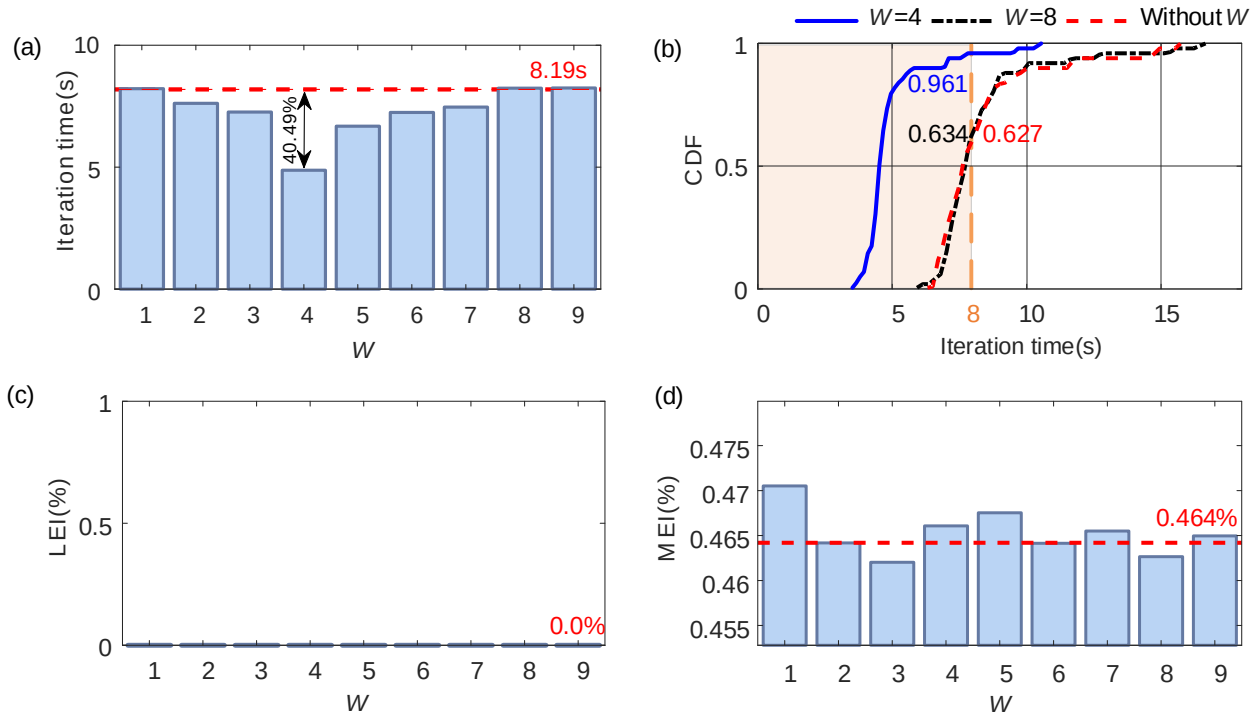


**Fig. 4.** Simulation results with different potential source numbers: (a) average iteration time, (b) CDF, (c) average LEI, and (d) average MEI.

To sum up, the proper selection of $W$ can reduce iteration time for generating acoustic maps, while maintaining solution accuracies in both source locations and strengths. This can be achieved especially when $W$ is in the vicinity of the actual source number. When errors exist in the estimation of $W$, the solving efficiency is no worse than the circumstance without $W$. Hence, the consideration of potential damage locations is useful to improve the computation efficiency of blade damage identification with the microphone array.

### 3.2 Effects of step-size shrinkage factors

Step-size shrinkage factor $\beta$ influences the step-size adjustment pattern, which controls the forward speed for finding appropriate solutions of damage identification. Moreover, a large value of $\eta^{(0)}$ can be set at the beginning of solving processes since the step-size is gradually scaled down by $\beta$ to guarantee convergence. Nevertheless, the selection criterion of $\beta$ is still undiscovered for

blade health assessment with the proposed method.

Effects of $\beta$ on acoustic source identification are investigated with 3600 Monte Carlo simulations, of which the microphone array and search grids are the same as the description in Section 3.1. Specifically, $\beta$ is changed from 0.1 to 0.9 with an interval of 0.05, and acoustic maps are also generated by the reference algorithm in which both backtracking and acceleration procedures are skipped. Simulation trials are run 200 times with each configuration. In addition, two randomly placed acoustic sources at 3000 Hz are considered to denote damages in wind turbine blades. The SNR in all simulations is 25 dB, and $W$ is set to 2. Furthermore, the initial step-size for conditions with $\beta$ is $10/\rho$ that is beyond the tolerance range mentioned in [27], and the fixed step-size $1/\rho$ is adopted in the reference algorithm to ensure the convergence.

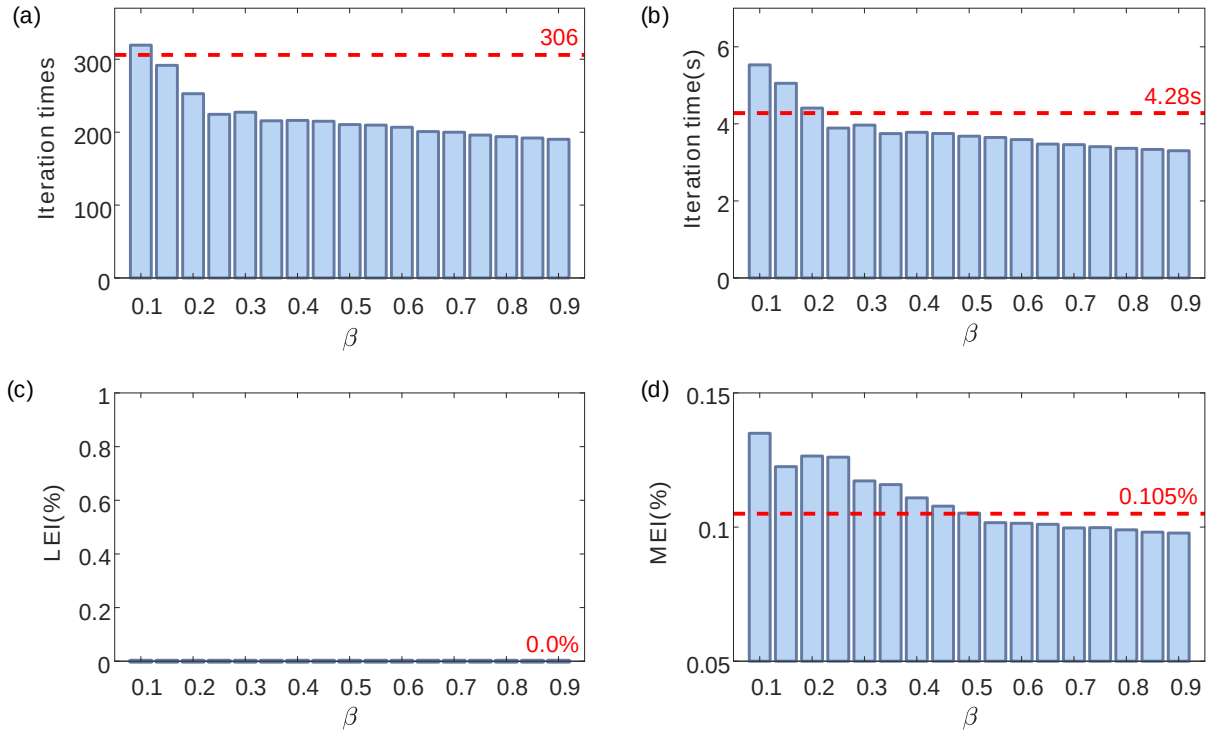


**Fig. 5.** Simulation results with different step-size shrinkage factors: (a) average iteration times, (b) average iteration time, (c) average LEI, and (d) average MEI.

It can be found in Fig. 5(a) and Fig. 5(b) that the increase in $\beta$ can cut down both average iteration times and computation time, leading to higher solving efficiency of acoustic inverse problems. With large values of $\beta$, the step-size in each iteration step is scaled moderately. In this circumstance, the solving procedure is efficiently performed with large step-sizes at preliminary stages. For later stages, outputs are finely adjusted with small step-sizes to ensure the accuracy of acoustic maps. Moreover, the efficiency of the proposed method can surpass that of the reference

condition, which is denoted as the red dotted line, when $\beta$ is larger than 0.2. On the contrary, the step-size adjustment is radical with small values of $\beta$. Then, step-sizes are too little at the early stage, leading to an increase in computation time. It is observed that average iteration times with $\beta$ = 0.15 and 0.2 are less than that of the reference, while more average iteration time is needed. This could be attributed to the additional computations induced by backtracking and acceleration processes. However, the increased time in each iteration can be hedged by the decrease in iteration times with large $\beta$. Besides, the localization accuracy is insensitive to the selection of $\beta$, and there is a trend that the average MEI increases slightly when $\beta$ decreases. This is probably because the solving procedure is stopped much earlier with smaller step-sizes.

Taken together, the adaptive adjustment strategy provides a valid approach to find appropriate step-sizes in computation processes, which can balance the efficiency and accuracy of blade damage identification. Thus, the difficulty in step-size determination for solving inverse problems with GMC penalties under variational conditions can be resolved. Moreover, it is preferable to set $\beta$ to relatively large values for the proposed method, which is beneficial to improve approximation abilities to the optimized step-size.

### 3.3 Effects of source frequencies

For active blade damage identification with the microphone array, loudspeakers are placed in blade cavities to make sounds, and analysis frequencies are selected as required. In addition, despite the great penetration of signals at low frequencies, the identification of low-frequency sources is still a challenging task. Therefore, this segment focuses on the effects of acoustic source frequencies on source identification performances of the proposed method.

Monte Carlo simulations are implemented with a microphone array and two randomly placed monopole sources, which are at frequencies from 2000 Hz to 8000 Hz with an interval of 1000 Hz. Simulation configurations are the same as the statement in Section 3.2. For each frequency, the proposed method and standard PGM developed in [27] are applied, and the SNR is 20 dB. Moreover, three values of step-size shrinkage factor $\beta$ = 0.6, 0.7, and 0.8 are considered, and the potential source number $W$ is set to 2. Furthermore, repeated trials are conducted 200 times with each simulation configuration.

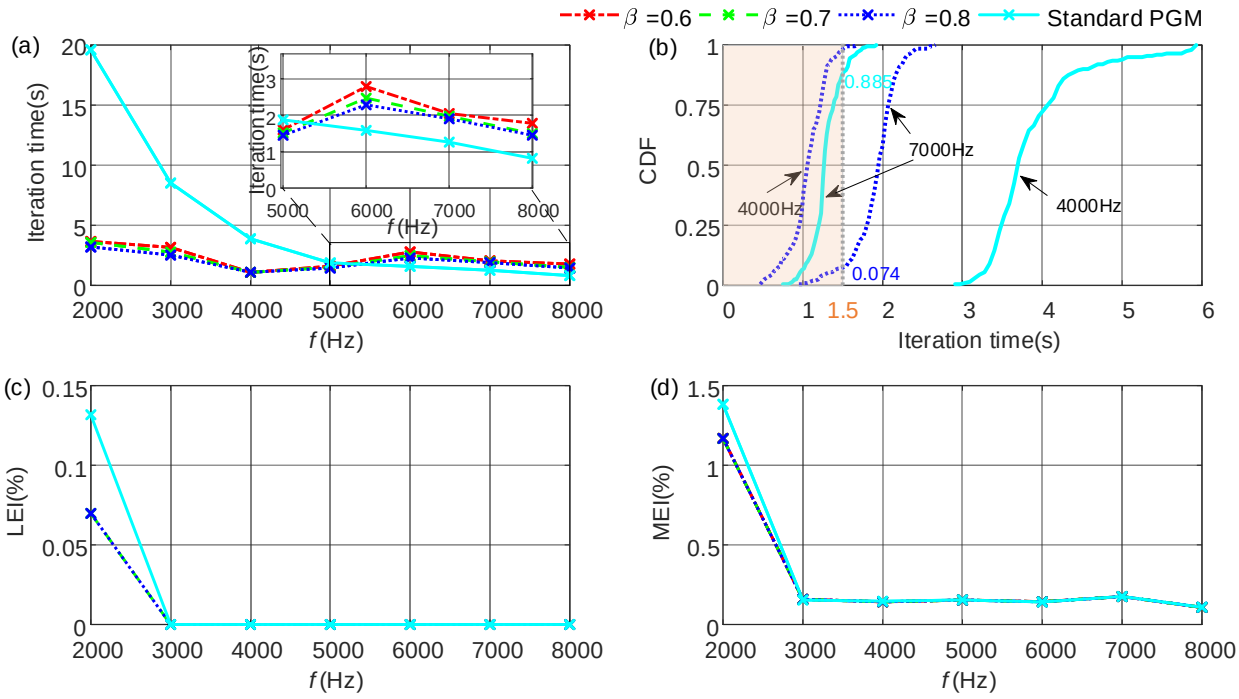


**Fig. 6.** Simulation results with different source frequencies: (a) average iteration time, (b) CDF, (c) average LEI, and (d) average MEI.

For the proposed method, curves in Fig. 6(a) with different $\beta$ are close to each other. In addition, patterns of average iteration time with two methods are different, and the distinction between them becomes inapparent with the increase in the source frequency. Specifically, the proposed method is more stable in solving efficiency than the standard PGM, and it could be induced by specially arranged initial solutions. These initial solutions provide a feasible way to approach the desired results by estimating potential damage locations. When the source frequency is lower than 6000 Hz, the proposed method is more efficient than the standard PGM. However, the proposed method is slower when the source frequency is no less than 6000 Hz, suggesting the limitation of the proposed method. Fig. 6(b) shows results from the view of the probability distribution. As for 4000 Hz, there is a great distance between CDF curves for different methods, and the minimal iteration time of standard PGM is larger than the maximum of the proposed method. When it comes to 7000 Hz, the proposed method performs slightly worse, and there are overlaps in the iteration time of the two methods. Moreover, Fig. 6(c) and Fig. 6(d) show that both localization and magnitude estimation accuracies of the proposed method are fine and stable within a wide range of source frequencies.

Results in this segment indicate that the proposed method can improve the solving efficiency of acoustic inverse problems under low-frequency circumstances while guaranteeing the accuracy

of acoustic maps. Moreover, poor performances induced by inappropriate estimations of step-sizes can be avoided by shrinking step-sizes adaptively. Therefore, it is preferable to detect blade damages with the excitation of loudspeakers at low frequencies, which is helpful to reduce economic costs and implementation difficulties of blade health management.

# 4. Validations based on experimental data

In this section, several experiments are conducted to examine the feasibility of blade damage identification based on the proposed method. Moreover, identification accuracy and efficiency for several types of damages are revealed by comparing results obtained using distinct approaches.

## 4.1 Experimental setup

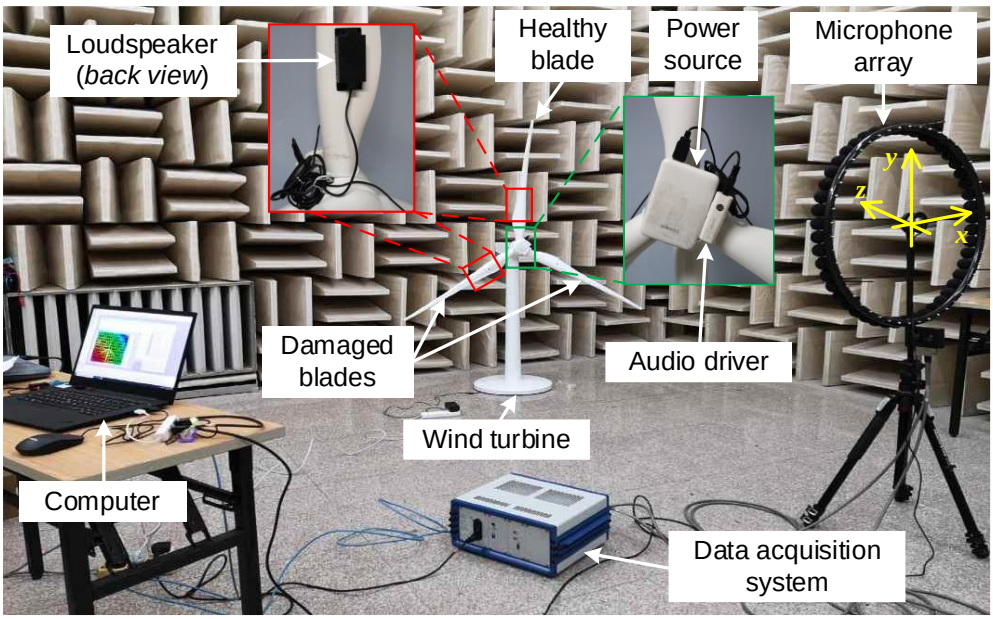


**Fig. 7.** Experimental setup for blade damage identification.

Experiments with a laboratory-scale wind turbine and microphone array were carried out in a semi-anechoic room. As shown in Fig. 7, the array was constituted by 48 microphones, and it was placed 2.15 m away from the blade rotation plane. Fig. 8 illustrates blades used in experiments, which were made of glass fiber reinforced plastics and had prefabricated openings for loudspeakers at the back. In addition, the wind turbine consisted of three blades, one of which was healthy, and the other two were damaged to simulate different health conditions, including blades with adhesive joint failures, cracks, and holes. Damages in blades were made by drills and cutters. In order to activate damage-related information for microphone array measurement, loudspeakers were installed in cavities of healthy and one of the damaged blades. Moreover, the wind turbine was driven by an electromotor at 10 rpm. It should be mentioned that the semi-anechoic room was used

to avoid the reverberation of rooms since actual wind turbines usually work in open areas where the sound reverberation is negligible.

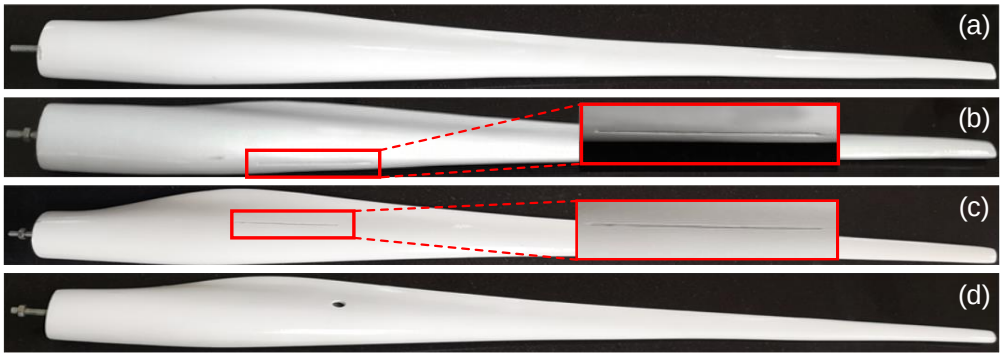


**Fig. 8.** Wind turbine blades used in experiments: (a) healthy blade, (b) damaged blade with an adhesive joint failure, (c) damaged blade with a crack, and (d) damaged blade with a hole.

### 4.2 Blade damage identification of adhesive joint failures

To examine the practicability of the proposed method, adhesive joint failures were simulated by thin kerfs with a length of 10 cm in the leading edge. Fig. 9 depicts acoustic maps for healthy and damaged blades with adhesive joint failures, and $\beta = 0.8$ and $W = 5$ are used for the proposed method. Search grids are at -1 m $< x <$ 1 m, -0.8 m $< y <$ 0.8 m, and the dynamic range is 10 dB. It should be stated that acoustic maps are rotated artificially based on the rotation center and speed, and the blur is insignificant due to the relatively slow rotation and short snapshot duration of 15 ms. It is depicted that adhesive joint failures are recognized by the proposed method, and the valid acoustic map can be seen in Fig. 9(a). There are several identified sources at the damaged blade with the loudspeaker, and damage locations can be reflected by source distributions. In addition, there is no source in another damaged blade and the healthy blade. Thus, it is feasible to examine blade health conditions with the microphone array, and damages can only be detected with loudspeakers in blade cavities.

For standard PGM and $l_1$-norm minimization, the sparsity of acoustic sources can be guaranteed in Fig. 9(b) and Fig. 9(c), whereas blade damages are not well recognized to provide useful information about blade damages. In this section, the step-size of standard PGM is set to $2/(3\rho)$ for all cases, and the selected step-size is not suitable to detect adhesive joint failures in wind turbine blades. The appropriate determination of step-sizes for standard PGM is a difficult task in blade damage identification, since there is little prior information that can be employed under variational conditions. In the proposed method, step-sizes in solving procedures of acoustic inverse

problems are adjusted adaptively to avoid improper selections, which is beneficial to improve the reliability of health assessment for actual blades. For conventional beamforming, the resolution of acoustic maps is too low to recover source distributions precisely, which is detrimental to feature extraction of blade damages.

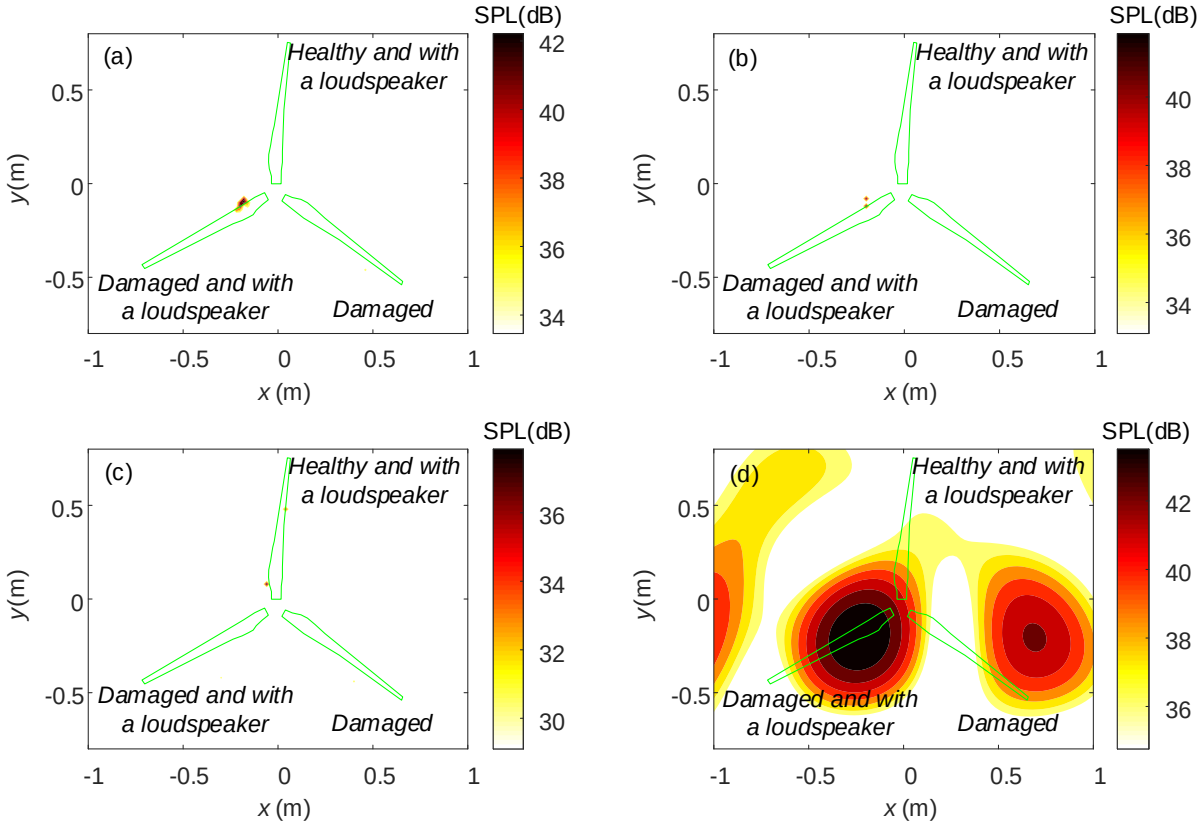


**Fig. 9.** Acoustic maps for healthy blades and blades with adhesive joint failures based on: (a) the proposed method, (b) standard PGM, (c) $l_1$-norm minimization, and (d) conventional beamforming.

It should be stated that there are flaws in damage identification results for adhesive joint failures based on the proposed method, and acoustic source locations are not completely corresponding to blade damages. This may be related to the opening direction of adhesive joint failures, and there is an obvious pressure gradient in the search plane. In addition, rotation compensation is also influential in acoustic maps due to inevitable errors about rotation speeds and initial angles in practical measurement. However, valuable information concerning adhesive joint failures can only be provided by the proposed method, and the other three methods are absolutely invalid for blade damage identification.

### 4.3 Blade damage identification of cracks

In experiments, cracks were represented by thin kerfs with a length of 10 cm at the pressure

side, with which sound transmission performances across blade walls were changed within a connected area. Additionally, shapes of cracks and adhesive joint failures were the same, and they existed in distinct parts of wind turbine blades.

As shown in Fig. 10(a), cracks can be recognized by the proposed method with $\beta = 0.8$ and $W = 5$, and there are several sources at the damaged blade with the loudspeaker. In addition, acoustic sources identified in the map are distributed in the damaged regions, which is useful for inferring blade damage locations and types. Fig. 10(b) to Fig. 10(d) are acoustic maps obtained by standard PGM, $l_1$-norm minimization, and conventional beamforming. Results based on standard PGM and the proposed method are extremely similar, indicating that there is little difference between identification accuracies of the two methods. Moreover, the computation time of the proposed method is 279.56 s, and it is significantly lower than that of standard PGM 523.16 s. In this context, the proposed method is more efficient for blade damage identification than the standard PGM, while result precisions based on the two methods are similarly fine.

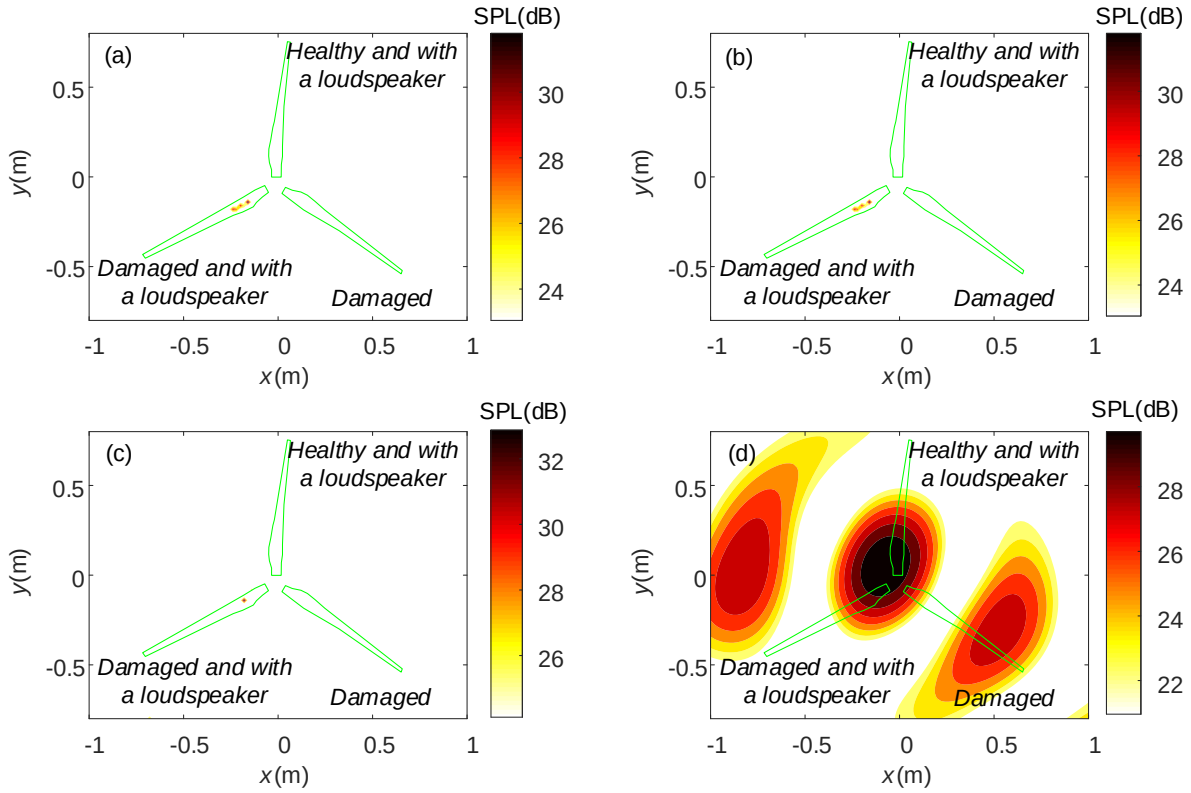


**Fig. 10.** Acoustic maps for healthy blades and blades with cracks based on: (a) the proposed method, (b) standard PGM, (c) $l_1$-norm minimization, and (d) conventional beamforming.

Results based on $l_1$-norm minimization are indeed sparse in the spatial domain, whereas the damage type is not well reflected in Fig. 10(c). The wrong recognition of distributed sources is a

common issue for $l_1$-norm minimization, and it is disadvantageous for examining blade health conditions in practical cases [35]. Conventional beamforming generates coarse and confusing results since it is not suitable for multiple source detection, especially with coherent sources. Hence, results based on $l_1$-norm minimization and conventional beamforming fail to provide valid information concerning cracks in wind turbine blades.

### 4.4 Blade damage identification of holes

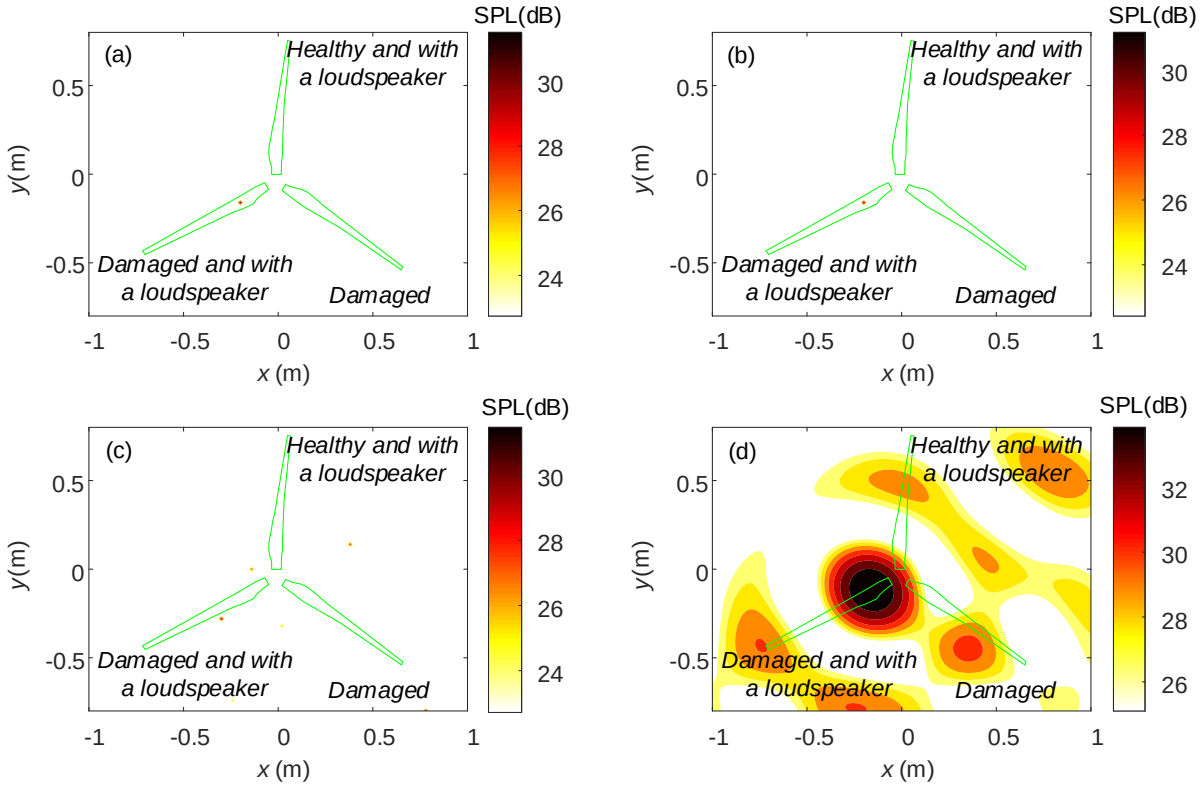


**Fig. 11.** Acoustic maps for healthy blades and blades with holes based on: (a) the proposed method, (b) standard PGM, (c) $l_1$-norm minimization, and (d) conventional beamforming.

In Fig. 11, holes in blades can be identified by the proposed method and the standard PGM, and source locations reflect damage positions in blades exactly. In this case, they are both feasible to generate accurate acoustic maps that are valuable for blade health management with the microphone array. However, the computation time of the standard PGM for identifying holes is 514.92 s, which is much higher than that of the proposed method 261.98 s. Fig. 11(c) shows the acoustic map obtained using $l_1$-norm minimization, in which acoustic sources can be found in both healthy and damaged blades. In addition, there is an identified source out of the blade structure. When it comes to conventional beamforming, although the acoustic source related to blade damages can be roughly found, the spatial resolution is extremely low to confuse damage locations.

Thus, acoustic maps obtained using $l_1$-norm minimization and conventional beamforming are inaccurate for blade damage identification.

The computation time of solving acoustic inverse problems under different conditions is illustrated in Fig. 12. For holes and cracks in wind turbine blades, they can be identified by both the proposed method and standard PGM with a constant step-size. Nevertheless, the computation time of standard PGM is too long to be used in practical applications, and the proposed method provides an effective way to accelerate the computation. When it comes to adhesive joint failures, valid information of blade damages cannot be provided by standard PGM due to the impropriety of step-sizes, and reliable identification results can be acquired by the proposed method effectively.

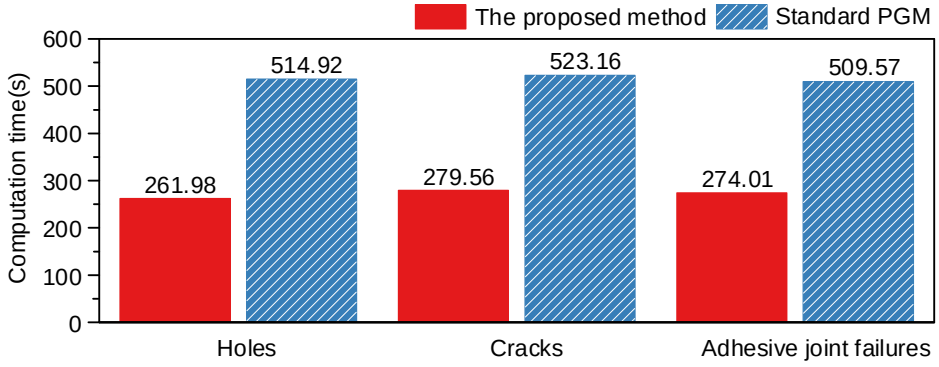


**Fig. 12.** Computation time for acoustic maps with different configurations.

To sum up, acoustic maps are convenient for recognizing blade damage locations and types based on source distributions, and the proposed method is applicable for blade damage identification with concentrated and distributed damages. Benefit from the designed algorithm, the difficulty of step-size determination in existing methods is resolved by adjusting step-sizes adaptively. In this context, blade damages can be reflected in high-resolution acoustic maps, and computation time for solving acoustic inverse problems with GMC penalties is cut down. Errors in identifying adhesive joint failures indicate that the proposed method is sensitive to all acoustic sources, which may disturb the identification precision of blade damages, especially with aerodynamic and mechanical noises. Thus, more advanced techniques for extracting damage-related sources need to be investigated in further studies.

## 5. Conclusions

This paper focuses on active damage identification of wind turbine blades with the microphone array, which is of great significance to improve the reliability of wind energy generation. An adaptive method for compressive beamforming based on the generalized minimax-

concave penalty function is proposed, and it can be used to identify blade damages by reconstructing sound fields with high spatial resolutions and efficiencies. Simulation results indicate that the method can overcome the difficulty in the step-size determination under variational conditions by adjusting step-sizes adaptively, and it performs well under low-frequency conditions. Besides, fast convergence can be achieved when the potential source number is close to the number of actual sources and the step-size shrinkage factor is relatively large. Moreover, the method is validated with a laboratory-scale wind turbine under different blade health conditions. Results show that blade damages can be recognized by the proposed method with great performances in computation efficiency and solution accuracy, and it is more practicable for damage identification of wind turbine blades than existing methods. This work provides a promising approach for blade health monitoring under operating conditions, and damage localization and classification are convenient to be achieved. For future research, the effects of wind and noise under operating conditions need to be considered, and studies with utility-scale wind turbines are necessary.

## Acknowledgements

This research was supported by National Natural Science Foundation of China under Grant No. 52075281 and 51975309. The valuable comments and suggestions from anonymous reviewers are highly appreciated.

## Abbreviations and Nomenclature

### Nomenclature

| | |
|---|---|
| $\boldsymbol{B}$ | Auxiliary matrix |
| $c$ | Velocity of sound, m/s |
| $\boldsymbol{d}$ | Peak index vector |
| $\boldsymbol{e}$ | Noise vector |
| $F$ | Objective function |
| $f$ | Items in the objective function |
| $\boldsymbol{G}$ | Propagation matrix |
| $g$ | Transfer function |
| $H$ | Generalized Huber function |
| $I$ | The number of actual acoustic sources |

| | |
|---|---|
| $k$ | Counting variable |
| $L$ | Lipschitz constant |
| $M$ | The number of microphones |
| $N$ | The number of search points |
| $\boldsymbol{p}$ | Sound pressure vector |
| **prox** | Proximal operator |
| $\boldsymbol{Q}$ | Rough acoustic map |
| $\hat{\boldsymbol{Q}}$ | Filtered acoustic map |
| $\boldsymbol{q}$ | Potential source strength vector |
| $\boldsymbol{q}^*$ | Actual strength vector |
| $R$ | The number of rows of acoustic maps |
| $\boldsymbol{r}$ | Position vector |
| $S$ | The number of columns of acoustic maps |
| $T$ | Threshold for element removal |
| $\boldsymbol{v}$ | Auxiliary vector |
| $W$ | The number of potential sources |
| $\boldsymbol{y}$ | Extrapolation point |
| $\nabla$ | Gradient of the function |

**Subscripts**

| | |
|---|---|
| $co$ | Copy |
| $l$ | The index of peaks |
| $m$ | The index of microphones |
| $n$ | The index of search points |
| $r$ | The row index of elements in acoustic maps |
| $s$ | The column index of elements in acoustic maps |
| $t$ | The index of iterations for step-size adjustment |

**Greek symbols**

| | |
|---|---|
| $\beta$ | Shrinkage factor |
| $\rho$ | Extrapolation parameter |

| | |
|---|---|
| $\sigma$ | Standard deviation |
| $\eta$ | Step-size |
| $\theta$ | Scale factor |
| $\lambda$ | Regularization parameter |
| $\mu$ | Mean |
| $\psi$ | GMC penalty function |
| $\omega$ | Angular frequency, rad/s |

**Abbreviations**

| | |
|---|---|
| CDF | Cumulative distribution function |
| GMC | Generalized minimax-concave |
| LEI | Location relative error index |
| MEI | Magnitude relative error index |
| PGM | Proximal gradient method |
| SNR | Signal-to-noise ratio |
| SPL | Sound pressure level |

# References


[1] H. Sun, H. Yang, Numerical investigation of the average wind speed of a single wind turbine and development of a novel three-dimensional multiple wind turbine wake model, Renew. Energ. 147 (2020) 192-203. https://doi.org/10.1016/j.renene.2019.08.122.

[2] Iea, Offshore Wind. https://www.iea.org/reports/offshore-wind, 2020 (accessed 2021-7-31 2021).

[3] Iea, Onshore Wind. https://www.iea.org/reports/onshore-wind, 2020 (accessed 2021-7-31 2021).

[4] P. Lux, A.G. Cassano, S.B. Johnson, M. Maiaru, S.E. Stapleton, Adhesive curing cycle time optimization in wind turbine blade manufacturing, Renew. Energ. 162 (2020) 397-410. https://doi.org/10.1016/j.renene.2020.08.043.

[5] L. Mishnaevsky, Repair of wind turbine blades: Review of methods and related computational mechanics problems, Renew. Energ. 140 (2019) 828-839. https://doi.org/10.1016/j.renene.2019.03.113.

[6] P. Tavner, How are we going to make offshore wind farms more reliable? Supergen Wind. (2011)

[7] Z. Lin, D. Cevasco, M. Collu, A methodology to develop reduced-order models to support the operation and maintenance of offshore wind turbines, Appl. Energ. 259 (2020) 114228. https://doi.org/10.1016/j.apenergy.2019.114228.

[8] D. Xu, P.F. Liu, Z.P. Chen, Damage mode identification and singular signal detection of composite wind turbine blade using acoustic emission, Compos. Struct. 255 (2021) 112954. https://doi.org/10.1016/j.compstruct.2020.112954.

[9] M.A. Oliveira, E.F. Simas Filho, M.C.S. Albuquerque, Y.T.B. Santos, I.C. Da Silva, C.T.T. Farias, Ultrasound-based identification of damage in wind turbine blades using novelty detection, Ultrasonics. 108 (2020) 106166. https://doi.org/10.1016/j.ultras.2020.106166.

[10] R. Yang, Y. He, H. Zhang, Progress and trends in nondestructive testing and evaluation for wind turbine composite blade, Renewable and Sustainable Energy Reviews. 60 (2016) 1225-1250. https://doi.org/10.1016/j.rser.2016.02.026.

[11] T. Wang, Q. Han, F. Chu, Z. Feng, Vibration based condition monitoring and fault diagnosis of wind turbine planetary gearbox: A review, Mech. Syst. Signal Pr. 126 (2019) 662-685. https://doi.org/10.1016/j.ymssp.2019.02.051.
[12] L. M., W. T., C. F., H. Q., Q. Z., J.Z. M., Scaling-Basis Chirplet Transform, IEEE T. Ind. Electron. 68 (2021) 8777-8788. https://doi.org/10.1109/TIE.2020.3013537.
[13] D. Tcherniak, L.L. Mølgaard, A. Güemes, Active vibration-based structural health monitoring system for wind turbine blade: Demonstration on an operating Vestas V27 wind turbine, Structural health monitoring. 16 (2017) 536-550. https://doi.org/10.1177/1475921717722725.
[14] M.D. Ulriksen, D. Tcherniak, L.M. Hansen, R.J. Johansen, L. Damkilde, L. Frøyd, In-situ damage localization for a wind turbine blade through outlier analysis of stochastic dynamic damage location vector-induced stress resultants, Structural Health Monitoring. 16 (2017) 745-761. https://doi.org/10.1177/1475921716681727.
[15] P. Zhu, J. Wu, M. Huang, X. Feng, H. Deng, H. Xie, M.A. Soto, Alternating strain response of fibre Bragg grating sensors embedded into carbon fibre composites for wind blade health monitoring, Seventh European Workshop on Optical Fibre Sensors, SPIE, Limassol, Cyprus, 2019.
[16] J. Lee, J. Park, K. Oh, S. Ju, J. Lee, Transformation algorithm of wind turbine blade moment signals for blade condition monitoring, Renew. Energ. 79 (2015) 209-218. https://doi.org/10.1016/j.renene.2014.11.030.
[17] S.A. Khoubrouy, J.H.L. Hansen, Microphone Array Processing Strategies for Distant-Based Automatic Speech Recognition, IEEE Signal Proc. Let. 23; 23 (2016) 1344-1348. https://doi.org/10.1109/LSP.2016.2592683.
[18] D. Salvati, C. Drioli, G. Ferrin, G.L. Foresti, Acoustic Source Localization From Multirotor UAVs, IEEE T. Ind. Electron. 67 (2020) 8618-8628. https://doi.org/10.1109/TIE.2019.2949529.
[19] P. Poozesh, K. Aizawa, C. Niezrecki, J. Baqersad, M. Inalpolat, G. Heilmann, Structural health monitoring of wind turbine blades using acoustic microphone array, Structural Health Monitoring. 16 (2017) 471-485. https://doi.org/10.1177/1475921716676871.
[20] C. Beale, M. Inalpolat, C. Niezrecki, Active acoustic damage detection of structural cavities using internal acoustic excitations, Structural Health Monitoring. 19 (2020) 48-65. https://doi.org/10.1177/1475921719835761.
[21] J. Billingsley, R. Kinns, The acoustic telescope, J. Sound Vib. 48 (1976) 485-510. https://doi.org/10.1016/0022-460X(76)90552-6.
[22] P. Chiariotti, M. Martarelli, P. Castellini, Acoustic beamforming for noise source localization – Reviews, methodology and applications, Mech. Syst. Signal Pr. 120 (2019) 422-448. https://doi.org/10.1016/j.ymssp.2018.09.019.
[23] A. Xenaki, P. Gerstoft, K. Mosegaard, Compressive beamforming, The Journal of the Acoustical Society of America. 136 (2014) 260-271. https://doi.org/10.1121/1.4883360.
[24] F. Ning, F. Pan, C. Zhang, Y. Liu, X. Li, J. Wei, A highly efficient compressed sensing algorithm for acoustic imaging in low signal-to-noise ratio environments, Mech. Syst. Signal Pr. 112 (2018) 113-128. https://doi.org/10.1016/j.ymssp.2018.04.028.
[25] H. Bu, X. Huang, X. Zhang, High-resolution Acoustical Imaging for Rotating Acoustic Source Based on Compressive Sensing Beamforming, 25th AIAA/CEAS Aeroacoustics Conference, Delft, The Netherlands, 2019.
[26] G. Battista, G. Herold, E. Sarradj, P. Castellini, P. Chiariotti, IRLS based inverse methods tailored to volumetric acoustic source mapping, Appl. Acoust. 172 (2021) 107599. https://doi.org/10.1016/j.apacoust.2020.107599.
[27] I. Selesnick, Sparse Regularization via Convex Analysis, IEEE T. Signal Proces. 65 (2017) 4481-4494. https://doi.org/10.1109/TSP.2017.2711501.
[28] S. Sun, T. Wang, F. Chu, A generalized minimax-concave penalty based compressive beamforming method for acoustic source identification, J. Sound Vib. 500 (2021) 116017. https://doi.org/10.1016/j.jsv.2021.116017.
[29] P.L. Combettes, J. Pesquet, Proximal splitting methods in signal processing, Fixed-point algorithms for inverse problems in science and engineering, Springer, New York, NY, 2011, pp. 185-212.

[30] H.H. Bauschke, P.L. Combettes, Convex analysis and monotone operator theory in Hilbert spaces, Springer, New York, NY, 2011.

[31] L. Condat, A Primal – Dual Splitting Method for Convex Optimization Involving Lipschitzian, Proximable and Linear Composite Terms, J. Optimiz. Theory App. 158 (2013) 460-479. https://doi.org/10.1007/s10957-012-0245-9.

[32] A. Beck, M. Teboulle, A fast iterative shrinkage-thresholding algorithm for linear inverse problems, SIAM J. Imaging Sci. 2 (2009) 183-202. https://doi.org/10.1137/080716542.

[33] Y. Nesterov, Gradient methods for minimizing composite functions, Math. Program. 140 (2013) 125-161. https://doi.org/10.1007/s10107-012-0629-5.

[34] D.P. Palomar, Y.C. Eldar, Convex optimization in signal processing and communications, Cambridge University Press, Cambridge, England, 2009.

[35] R.M. Levine, Ultrasonic guided wave imaging via sparse reconstruction, Georgia Institute of Technology, 2014.